

MULTI-POLARIZED MICROWAVE POWER IMAGING ALGORITHM FOR EARLY BREAST CANCER DETECTION

W. Shao* and R. S. Adams

Department of Electrical and Computer Engineering, University of North Carolina at Charlotte, 9201 University City Blvd, Charlotte, NC 28262, USA

Abstract—A new image reconstruction algorithm for early breast cancer detection using ultra-wideband microwave signals is proposed. In this algorithm, the backscattered electric and magnetic fields are measured and combined in a novel way; the direction of power flow with respect to a given focal point is used to localize tumors. Significant improvement in signal-to-mean ratio (SMR) and signal-to-clutter ratio (SCR) are achieved when driving signals consist of waves with multiple polarizations. Numerical results demonstrate nearly 5.5 dB improvement of SMR and SCR over the traditional Confocal Microwave Imaging method when a single 8 mm breast tumor is present.

1. INTRODUCTION

Breast cancer is the most common form of cancers among women. In 2011, an estimated 230,480 new cases of invasive breast cancer were expected to be diagnosed in women in the U.S., along with 57,650 additional cases of in situ breast cancer [1]. In addition, approximately 39,520 women in the U.S. were estimated to die from breast cancer within that year [1]. To reduce the mortality of this disease, it is imperative that it be detected early when the cancer is relatively small and has not spread to other parts of the body. The current leading method of detection for this type of cancer is mammography in which the breast is exposed to low-power X-rays and a resultant image is formed. Unfortunately, this method is fraught with problems such as high false negative rates [2], high false positive rates [3], and the

Received 25 August 2011, Accepted 13 January 2012, Scheduled 20 January 2012

* Corresponding author: Wenyi Shao (wshao1@uncc.edu).

ionizing nature of X-rays which poses a considerable risk of causing the very cancer it attempts to detect. To date, no mainstream method has been developed that provides a safer and/or more accurate method than traditional mammography.

More than a decade ago, Hagness et al. [4] proposed an alternative method of breast cancer detection; ultra wideband microwave signals were used to create a three-dimensional image of the breast. This approach is appealing since microwave signals are non-ionizing and thus it is much safer for a patient to undergo such a scan without increasing the risk of cancer development. For this approach to become a viable complement to, or replacement for, mammography, many technical and theoretical challenges must be overcome. For instance, wideband signals require very narrow width pulses in the time domain, the generation of which requires high performance antennas, impedance matching networks, signal sources, etc.. In addition to the need for hardware design, an efficient and effective near field image reconstruction algorithm is necessary — this latter topic is the motivation of the ensuing work.

The dielectric properties of healthy breast tissue, and that of malignant tumors, differ significantly at microwave frequencies [5–9]. The most recent research shows that dielectric properties contrast between malignant breast tissues and normal adipose-dominated breast tissues ranges up to 10:1 [8]. Therefore, an inverse scattering method that constructs images by recovering the permittivity or conductivity profile of the breast is a feasible approach to detect cancerous growth. Examples of such methods are diffraction tomographic (DT) algorithm [10], Born approximation (BA) [11], Born iterative method (BIM) [12] and distorted BIM (DBIM) [13]. These methods were originally developed for ground penetrating radar (GPR) but some have been effectively applied in the area of breast cancer medical imaging [14].

The problem of 3-D microwave medical imaging differs from that of GPR in that rapid (ideally real time) results are required for effective diagnosis. Since the inverse methods such as those listed above are usually inefficient, other methods are necessary to provide more rapid results. One such approach is confocal microwave imaging (CMI) [15], also called Delay-and-Sum (DAS). DAS only focuses on reflections from scatterers but avoids estimating the dielectric properties of the whole area. As the illuminating signal is an ultrawideband pulse, this translates to simply time shifting and summing signals. As an extension of DAS, the improved-DAS (IDAS) [17] uses an additional weight factor that essentially represents the preprocessing and coherent radar operation, calculated at each focal point to improve image

quality. Delay-Multiply-and-Sum (DMAS) is another approach in the DAS family, in which the time-shifted signals are multiplied in pair before summing [16]. Its authors have shown an approximately 5 dB \sim 8 dB improvement in signal-to-mean ratio (SMR) and 1.25 dB \sim 3.1 dB improvement in signal-to-clutter ratio (SCR) over DAS through investigating a simple rectangular breast model. DAS and its follow-up algorithms have shown to be very efficient approaches with acceptable image contrast and resolution.

In this paper, a new image reconstruction algorithm-microwave power imaging (MPI), is presented that applies electric backscattered signals as well as magnetic backscattered signals. These signals are time shifted and then combined to compute a Poynting like signal before summing to create a focal point. This algorithm has an equivalent efficiency to DAS but with higher image quality. An MRI-derived numerical breast phantom is applied to verify the proposed algorithm. Multi-polarized detecting signals are also applied in the proposed approach to further improve the image quality [18]. Numerical results show that the proposed method can detect breast tumors as small as 8 mm in diameter with high contrast.

In Section 2, the MPI algorithm is described in detail, Section 3 introduces the multi-polarized detecting system simulated by the FDTD method, and Section 4 provides numerical results and comparisons to DMAS and DAS. The conclusion is summarized in Section 5.

2. MICROWAVE POWER IMAGING (MPI) ALGORITHM

It is desired to improve the efficacy of the multistatic confocal microwave imaging algorithm [19] by including the magnetic field with the electric field in the formulation. To do so, we have chosen to combine the two fields into a Poynting like vector that represents the magnitude and direction of power flow within the system. At any point in Cartesian space, the Poynting vector is given by

$$\begin{aligned} \mathbf{P} &= \mathbf{E} \times \mathbf{H} = \begin{vmatrix} \hat{x} & \hat{y} & \hat{z} \\ E_x & E_y & E_z \\ H_x & H_y & H_z \end{vmatrix} \\ &= (E_y H_z - E_z H_y) \hat{x} + (E_z H_x - E_x H_z) \hat{y} + (E_x H_y - E_y H_x) \hat{z} \\ &= P_x \cdot \hat{x} + P_y \cdot \hat{y} + P_z \cdot \hat{z} \end{aligned} \quad (1)$$

where $P_x = E_y H_z - E_z H_y$, $P_y = E_z H_x - E_x H_z$, and $P_z = E_x H_y - E_y H_x$. All the electric and magnetic field signals are assumed have been time

shifted, except where otherwise noted. The time shifting process has been described in numerous publications [16, 19, 20]. Note that for the multistatic mode, time delay compensation is only required from the focal point to the detector. The signal propagation velocity within the breast in our investigation is equivalent to a wave traveling in a medium that has relative dielectric constant $\epsilon_r = 5.7$ and conductivity $\sigma = 0.16$ m/s — very close to the dielectric properties of fatty breast tissue.

At any instant in time, a single antenna operates in transmit mode and many other antennas receive the response to that transmitted signal. If the transmitted electric field is polarized along the y -direction, only P_x and P_z at the receivers are likely provide meaningful results. If the z -direction is assumed to point away from the body, then P_z contains reflections from the tumor as well as significant reflections from the muscle layer beneath the breast (a more detailed description of the breast model used for validation will be presented in Section 3). So for the proposed algorithm, P_x is the only term that can be reasonably used to detect the tumor with y -polarized excitation. The first term of P_x dominates over the second term, again because of the polarization of excitation. Thus the x -component of the received Poynting vector is well-approximated with

$$P_x \approx E_y H_z \quad (2)$$

From a similar line of reasoning, an x -polarized excitation signal gives

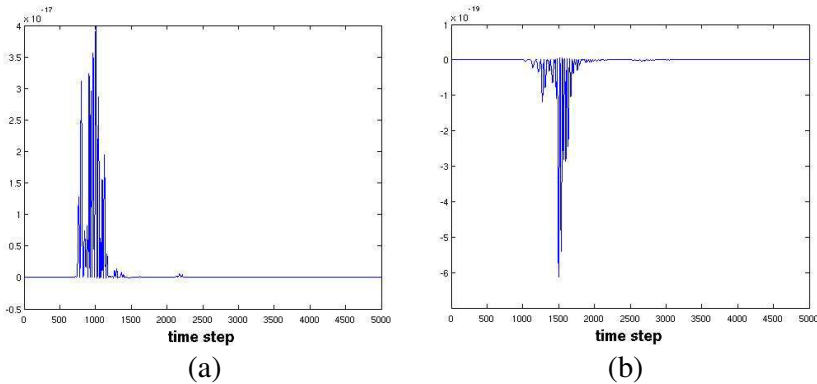


Figure 1. The product of E_y field and H_z field at a given receiver may be either (a) exclusively positive, if the receiver is located in the positive x -direction from a tumor, or (b) exclusively negative if the receiver is located in the negative x -direction from a tumor.

rise to P_y that is well approximated with

$$P_y \approx -E_x H_z \tag{3}$$

The traditional CMI algorithm sums signals coherently at each target location after time delay compensation since the phase front of E_y is spherically symmetric. However, the phase front of H_z is spherically antisymmetric about the Y - Z plane, in which the tumor is located. Therefore, Equation (2) at receiver locations in the positive x direction from the tumor is positive for all time; Equation (2) at receiver locations in the negative x direction from the tumor is negative for all time. This problem is depicted in Figure 1 for a receiver in the positive and negative x -direction from a tumor. Since a negative result represents power flow in the negative direction, the total power reflected from a given focal point can be deduced if each receiver in the negative x -direction of the current focal point is multiplied by -1 , or

$$P_{xij} = \begin{cases} E_{yi} H_{zj} & x_R > x_F \\ -E_{yi} H_{zj} & x_R < x_F \end{cases} \tag{4}$$

where $i, j = 1 \sim N$ (N is the total number of receivers), x_R is the x coordinate of the j th receiver and x_F is the x coordinate of the current focal point. At this stage, it is worth noting that the position of each detector has been taken into account in the proposed algorithm and participates in the intensity computation of each focal point (for DAS, IDAS or DMAS, only the transit time of the signal from the focal point to the detector is considered). Hence, when the x coordinate of the detector lies between the tumor and the current focal-point, the x -directed power obtained from these detectors are entirely inverted. This will further suppress the background noise of the image and improve image quality. Finally, these time-shifted products are summed to yield the intensity value of the focal point according to

$$\begin{aligned} I(\vec{r}) &= \int_0^T \left(E_{y1} H_{z1}^r + E_{y1} H_{z2}^r + \dots + E_{y1} H_{zN}^r \right. \\ &\quad \left. + E_{y2} H_{z1}^r + E_{y2} H_{z2}^r + \dots + E_{y2} H_{zN}^r \right. \\ &\quad \left. + \vdots \right. \\ &\quad \left. + E_{yN} H_{z1}^r + E_{yN} H_{z2}^r + \dots + E_{yN} H_{zN}^r \right) dt \\ &= \int_0^T \left[\sum_{i=1}^N E_{yi} \cdot \sum_{j=1}^N H_{zj}^r \right] dt = \int_0^T \left(\sum_{i,j=1}^N P_{xij} \right) dt \tag{5} \end{aligned}$$

where \vec{r} is the position of the synthetic focal point in 3D Cartesian space, $H_{zj}^r = H_{zj}$ when $x_R > x_F$, $H_{zj}^r = -H_{zj}$ when $x_R < x_F$, and T is the total measurement time. Note that P_{xii} is the actual Poynting vector associated with the i th pixel location; P_{xij} ($i \neq j$) is a fictitious cross term that contributes to the focal point intensity but has no physical meaning.

Equation (5) clearly illustrates that the number of E field and H field detectors need not be identical, nor must they be collocated. If M is the number of E field detectors and N is the number of H field detectors, then the intensity is given by

$$I(\vec{r}) = \int_0^T \left[\sum_{i=1}^M E_{yi} \cdot \sum_{j=1}^N H_{zj}^r \right] dt \quad (6)$$

Thus E_y and H_z may be processed separately. This observation eases the burden of collecting these field components in a physical measurement since each detecting antenna may be optimized to detect either E_y or H_z , but not necessarily both.

To conclude the formulation, the intensity of an x -polarized electric excitation signal from Equation (3) is computed as

$$I(\vec{r}) = \int_0^T \left(\sum_{i,j=1}^N P_{yij} \right) dt = \int_0^T \left[- \sum_{i=1}^M E_{xi} \cdot \sum_{j=1}^N H_{zj}^r \right] dt \quad (7)$$

$$\text{where, } H_{zj}^r = \begin{cases} H_{zj} & y_R > y_F \\ -H_{zj} & y_R < y_F \end{cases}.$$

3. FDTD SIMULATION AND MULTI-POLARIZED DETECTION

To easily illustrate the salient features of the proposed scheme, the FDTD method is employed in this analysis to simulate the electromagnetic response of a scattered fibroglandular breast model derived from the University of Wisconsin MRI numerical breast phantoms repository [21]. In this analysis, a total of four simulations are used and in each only one transmitter (point source) is excited; the transmitters, positioned external to the breast phantom as shown in Figure 2, are polarized in the $-x$, $+y$, $+x$ and $-y$ direction respectively. Each transmitting dipole is located 2 millimeters from the surface of the skin and is excited in succession. The entire breast phantom was immersed in a coupling medium, whose relative dielectric constant is 5.7 and conductivity is zero.

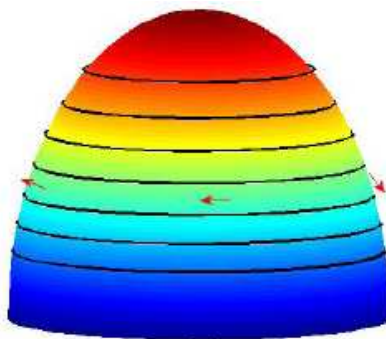


Figure 2. 56 receivers lie along 7 circles — each has 8 receivers (receivers not illustrated in this figure). Four transmitters (in red arrows) illuminate the breast successively from different positions, polarized along $-x$, $+y$, $+x$ and $-y$ respectively.

Fifty six receivers are positioned around the breast model on the surface of the skin in seven layers — along the black circles shown in Figure 2. Each receiver is assumed to be located in the center of its respective Yee cell [22]. Hence, in the Yee cell, the E field signal requires four point averaging and the H field signal requires two-point averaging:

$$E_x = \frac{1}{4} \left[E_x \left(i + \frac{1}{2}, j, k \right) + E_x \left(i + \frac{1}{2}, j + 1, k \right) + E_x \left(i + \frac{1}{2}, j, k + 1 \right) + E_x \left(i + \frac{1}{2}, j + 1, k + 1 \right) \right] \quad (8)$$

$$H_x = \frac{1}{2} \left[H_x \left(i, j + \frac{1}{2}, k + \frac{1}{2} \right) + H_x \left(i + 1, j + \frac{1}{2}, k + \frac{1}{2} \right) \right] \quad (9)$$

Equations for E_y , E_z , H_y , and H_z are similar.

The grid size used in this 3-D FDTD model is $\Delta x = \Delta y = \Delta z = 0.5$ mm and the time step is $\Delta t = \frac{4}{3}$ ps. The computational space is terminated with a second-order Liao absorbing boundary [23]. The UWB transmitted signal is comprised of a modulated Gaussian pulse with spectrum peak at 6.25 GHz and 3 dB bandwidth of 10 GHz. The computational time for one transmission, and allowing for the backscattered signals to be received at the antenna array (5000 time steps) is approximately 6 hours by serial fortran code on state of the art linux servers; one simulation consists of four transmissions and collections due to multi-polarized sources. Thus, 4×56 series of data are involved in the signal processing. The final intensity value

of the synthetic focal point is the summation of values obtained by Equations (5) and (7) from 4 illuminations,

$$I(\vec{r}) = \int_0^T \left(\sum_{i,j=1}^N P_{x1}^{ij} + \sum_{i,j=1}^N P_{y1}^{ij} + \sum_{i,j=1}^N P_{x2}^{ij} + \sum_{i,j=1}^N P_{y2}^{ij} \right) dt \quad (10)$$

where $N = 56$. Note that the intensity of some focal points calculated by Equation (10) is likely negative. When this happens all intensity values are normalized to lie between zero and one.

The signals presented to the receivers are comprised of instant wave, scattered wave from the skin and muscle and other clutter objects, as well as the response from the tumor. Usually, the tumor's response can be extracted by subtracting a reference model which is an indential but tumor-free model. Since a regular tomography examination is recommended at least once each year [24], the previous examination data can be reasonably used as reference data. Considering tissue properties may vary over time, in our investigation the breast phantom containing a tumor has $\pm 10\%$ random variation (in dielectric constant as well as conductivity for each cell) from the tumor-free model. This method helps us to easily obtain the tumor response for performance analysis of the proposed algorithm. A more practical approach in real experiments to obtain tumor response may be found in [25].

4. NUMERICAL RESULTS

4.1. Single Tumor

In this section, a 8 mm diameter tumor was inserted into the breast phantom to investigate the quality of the proposed MPI algorithm, compared to a DMAS, and DAS using the same antenna scheme. Figure 3 compares their reconstructed results in the transverse plane (X - Y plane), coronal plane (Y - Z plane) and sagittal plane (X - Z plane). Intensity outside of the breast-phantom area (coupling-liquid area) was set to zero. Clearly, figures obtained by multi-polarized MPI provide the best image. The tumor, centered at (78, 75, 50) in the simulated space, is clearly illustrated at the correct location. It is interesting to note that clutters observed in DMAS are occasionally stronger than DAS; image contrast of DMAS is generally improved over DAS. This will be discussed further in the following section.

To make a quantitative assessment, the intensity ratio of the strongest focal point against the mean background SMR, and against the maximum clutter response SCR are computed to investigate the

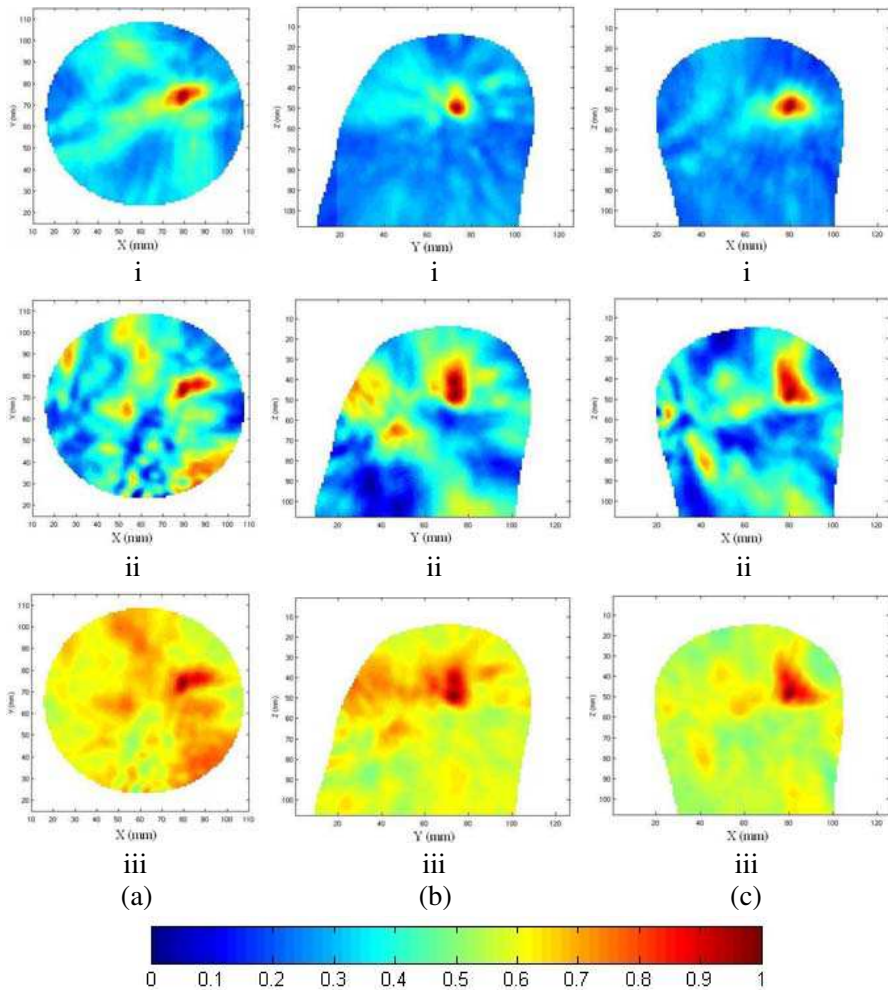


Figure 3. Comparison of reconstructed images in (a) $x-y$ plane, (b) $z-y$ plane, and (c) $z-x$ plane by three approaches: (i) MPI; (ii) DMAS. (iii) DAS. Diameter of the tumor is 8 mm for all cases.

contrast of each image. The SMR and SCR value for Figure 3 are shown in Table 1. For all views, the SMR and SCR values for MPI is the highest among the three.

Figure 4 shows the reconstructed image using MPI when the tumor-contained breast phantom and the tumor-free breast phantom have $\pm 15\%$ difference in dielectric parameters. The image quality is much worse than the $\pm 10\%$ case though the tumor is still able to be

Table 1. Comparison of SMR and SCR value for Figure 3.

Figure number	Method	SMR (dB)	SCR (dB)
Figure 3(a)i	MPI	5.311	2.001
Figure 3(a)ii	DMAS	3.936	1.098
Figure 3(a)iii	DAS	1.919	0.999
Figure 3(b)i	MPI	5.343	3.280
Figure 3(b)ii	DMAS	4.187	0.067
Figure 3(b)iii	DAS	2.375	1.650
Figure 3(c)i	MPI	5.680	1.768
Figure 3(c)ii	DMAS	4.435	1.327
Figure 3(c)iii	DAS	2.099	0.285

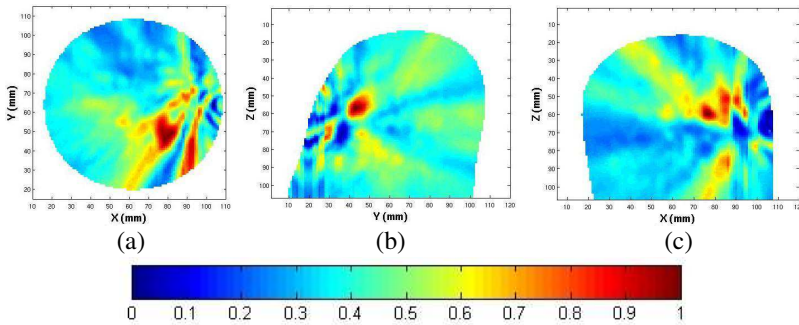


Figure 4. Reconstructed image for tumor centered at $(78, 45, 60)$ with 8mm diameter using MPI. Tumor-contained breast phantom and the tumor-free breast phantom are $\pm 15\%$ randomly different in dielectric parameters. (a) in the x - y plane, (b) in the z - y plane, and (c) in the z - x plane.

recognized centered in $(78, 45, 60)$. Neither DAS nor DMAS is able to locate the target in this scenario.

4.2. Dual Tumor

The dual-tumor case is used to investigate resolution of the proposed imaging method. In general, imaging resolution is defined by the minimal distance between two targets at which the two targets can still be distinguished in the reconstructed image. Typically, it can be characterized by a -3 dB point of the power level in the reconstructed image. In this section, we study both the horizontal and vertical

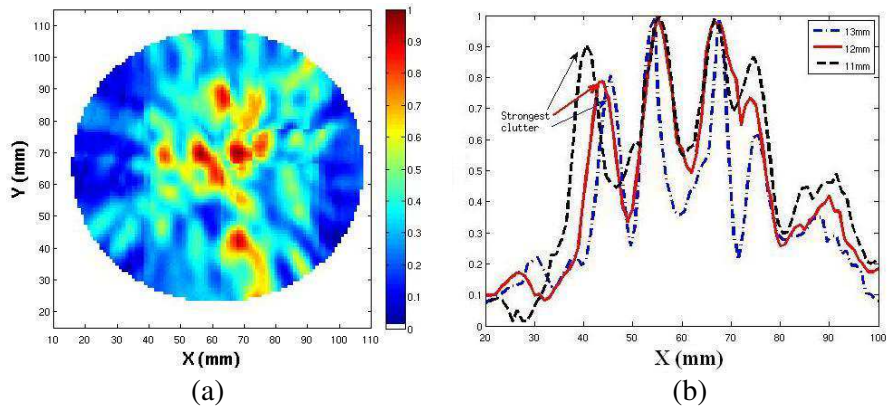


Figure 5. Two-tumor prototype for study of horizontal resolution. (a) is the reconstructed image when two tumors are 12 mm apart. Center positions are (56, 70, 50) and (68, 70, 50). (b) shows the intensity along the line $y = 70$ in the plane of $z = 50$ when two tumors are 11 mm, 12 mm, and 13 mm apart.

imaging resolution of the proposed algorithm as an illustration of the detection and imaging of a spherical pair of tumors, each of 6 mm diameter, using the breast phantom and antenna scheme depicted in Section 3. The breast phantoms with and without tumors differ with $\pm 10\%$ random variation.

The horizontal plane resolution is determined by analyzing the distance between two identical targets placed in the center of the x - y plane. Figure 5(a) shows the reconstructed image when two targets are centered at (56, 70, 50) and (68, 70, 50), a 12 mm offset. It is difficult to identify the tumors in this image since clutters are very strong. Figure 5(b) illustrates the intensity of the focal points along the line $y = 70$ in the reconstructed plane when two tumors are 11 mm, 12 mm, or 13 mm apart. This figure demonstrates that the resolution of the proposed reconstruction approach is near 12 mm in the horizontal plane. This translates to approximately 0.6λ at the peak-spectrum frequency, and approximately 0.1λ at the lower edge frequency (1 GHz) of the UWB signal in the coupling medium. Figure 5 also implies that clutters in the 11 mm-apart case (black dash line) would be even stronger than the 12 mm-apart and 13 mm-apart case.

Similarly, the vertical resolution is studied by varying the distance between two identical tumors, placed in the z - y plane. Figure 6(a) shows the reconstructed image when two 6 mm-diameter tumors centered at (75, 75, 59) and (75, 75, 63). Hence center distance is

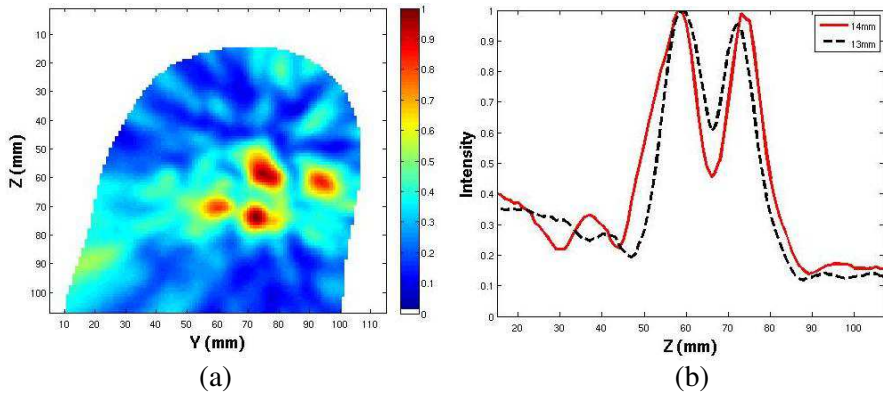


Figure 6. Two-tumor prototype for study of vertical resolution. (a) is the reconstructed image when two tumors are 14 mm apart. Center positions are $(75, 75, 59)$ and $(75, 75, 73)$. (b) shows the intensity along the line $y = 75$ in the $z-y$ plane of $x = 75$ when two tumors are 13 mm, and 14 mm apart.

14 mm. Clutters are observed to be strong in the image, however two tumors can be clearly identified and distinguished. Figure 6(b) illustrates the intensity of the focal points along the line $y = 75$ in the reconstructed plane when two tumors are 13 mm or 14 mm apart. This figure demonstrates that at a distance of 14 mm, two tumors are able to be distinguished. This is equivalent to approximately 0.7λ at the peak-spectrum frequency of the UWB detecting signal and 0.112λ at 1 GHz in the coupling medium.

5. CONCLUSION

A new, fast, multi-polarized MPI algorithm is proposed to detect early stage breast cancer. In this algorithm, four electric excitations, polarized along $+y$, $+x$, $-y$, $-x$, respectively, are used to transmit an ultra-wideband pulse, and an aperture array is used for data collection. Both electric and magnetic field backscattered signals extracted from FDTD simulations are applied to compute a Poynting type signal and finally reconstruct an image. It has been demonstrated that the proposed algorithm is able to detect small (6 mm in diameter) tumors. Comparison of reconstructed images obtained by multi-polarized MPI, DMAS and DAS were presented. The results show that multi-polarized MPI provides the highest contrast of all approaches analyzed with good image resolution. Numerical simulations have verified the above conclusions.

REFERENCES

1. American Cancer Society, *Breast Cancer Facts Figures 2011–2012*, Nov. 2011. Available on www.cancer.org/Research/CancerFactsFigures/BreastCancerFactsFigures.
2. Huynh, P. T., A. M. Jarolimek, and S. Daye, “The false-negative mammogram,” *Radiograph.*, Vol. 18, No. 5, 1137–1154, 1998.
3. Elmore, J. G., M. B. Barton, V. M. Mocerri, S. Polk, P. J. Arena, and S. W. Fletcher, “Ten-year risk of false positive screening mammograms and clinical breast examinations,” *New Eng. J. Med.*, Vol. 338, No. 16, 1089–1096, 1998.
4. Hagness, S. C., A. Taflove, and J. E. Bridges, “Two-dimensional FDTD analysis of a pulsed microwave confocal system for breast cancer detection: Fixed-focus and antenna-array sensors,” *IEEE Trans. Biomed. Eng.*, Vol. 45, 1470–1479, Dec. 1998.
5. Surowiec, A. J., S. S. Stuchly, J. R. Barr, and A. Swarup, “Dielectric properties of breast carcinoma and the surrounding tissues,” *IEEE Trans. Biomed. Eng.*, Vol. 35, 257–263, Apr. 1988.
6. Joines, W. T., Y. Zhang, C. Li, and R. L. Jirtle, “The measured electrical properties of normal and malignant human tissues from 50 to 900 MHz,” *Med. Phys.*, Vol. 21, 547–550, Apr. 1994.
7. Chaudhary, S. S., R. K. Mishra, A. Swarup, and J. M. Thomas, “Dielectric properties of normal and malignant human breast tissues at radiowave and microwave frequencies,” *Indian J. Biochem. Biophys.*, Vol. 21, 76–79, Feb. 1984.
8. Lazebnik, M., D. Popovid, L. McCartney, C. Watkins, M. Lindstrom, J. Harter, S. Sewall, T. Ogilvie, A. Magliocco, T. Breslin, W. Temple, D. Mew, J. Booske, M. Okoniewski, and S. Hagness, “A large-scale study of the ultrawideband microwave dielectric properties of normal, benign and malignant breast tissues obtained from cancer surgeries,” *Phys. Med. Biol.*, Vol. 52, 6093–6115, 2007.
9. Lazebnik, M., L. McCartney, D. Popovic, C. B. Watkins, M. J. Lindstrom, J. Harter, S. Sewall, A. Magliocco, J. H. Booske, M. Okoniewski, and S. C. Hagness, “A large-scale study of the ultrawideband microwave dielectric properties of normal breast tissue obtained from reduction surgeries,” *Phys. Med. Biol.*, Vol. 52, 2637–2656, 2007.
10. Cui, T. and W. Chew, “Diffraction tomographic algorithm for the detection of three-dimensional objects buried in a lossy half-space,” *IEEE Trans. Antennas and Propagation*, Vol. 50, No. 1, 42–49, Jan. 2002.

11. Born, M. and E. Wolf, *Principles of Optics*, 6th edition, Pergamon Press, New York, 1980.
12. Moghaddam, M., W. C. Chew, and M. Oristaglio, "Comparison of the born iterative method and Tarantola's method for an electromagnetic time-domain inverse problem," *Int. J. Imag. Sys. Tech.*, Vol. 3, No. 4, 318–333, 1991.
13. Chew, W. and Y. Wang, "Reconstruction of two-dimensional permittivity distribution using the distorted Born iterative method," *IEEE Trans. Med. Imaging*, Vol. 9, No. 2, 218–225, Jun. 1990.
14. Winters, D. W., J. D. Shea, P. Kosmas, B. D. van Veen, and S. C. Hagness, "Three-dimensional microwave breast imaging: Dispersive dielectric properties estimation using patient-specific basis functions," *IEEE Trans. Med. Imaging*, Vol. 28, No. 7, 969–981, Jul. 2009.
15. Fear, E., X. Li, S. C. Hagness, and M. Stunchly, "Confocal microwave imaging for breast cancer detection: Localization of tumors in 3 dimensions," *IEEE Trans. Biomed. Eng.*, Vol. 49, No. 8, 812–822, 2002.
16. Lim, H. B., N. T. T. Nhung, E. Li, and N. D. Thang, "Confocal microwave imaging for breast cancer detection: Delay-multiply-and-sum image reconstruction algorithm," *IEEE Trans. Biomed. Eng.*, Vol. 55, No. 6, 1697–1704, 2008.
17. Klemm, M., I. J. Craddock, J. A. Leendertz, A. Preece, and R. Benjamin, "Improved delay-and-sum beamforming algorithm for breast cancer detection," *Int. Journal of Ant. and Prop.*, Vol. 2008, 9, Article ID 761402, 2008, doi:10.1155/2008/761402.
18. Shao, W. and R. Adams, "UWB imaging with multi-polarized signals for early breast cancer detection," *Proceedings of the 2010 IEEE Ant. and Prop. Society International Symposium*, 1–4, 2010.
19. Shao, W., B. Zhou, and G. Wang, "UWB microwave imaging for early detection of breast cancer," *Journal of Microwaves*, Vol. 21, No. 3, 64–67, 2005, in Chinese.
20. Li, X. and S. Hagness, "A confocal microwave imaging algorithm for breast cancer detection," *IEEE Microwave and Wireless Components Lett.*, Vol. 11, No. 3, 130–132, 2001.
21. The UWCEM Numerical Breast Phantoms Repository. Available at <http://uwcem.ece.wisc.edu/MRI/database/>.
22. Yee, K., "Numerical solution of initial boundary value problems involving Maxwell's equation in isotropic media," *IEEE Trans. Antennas and Propagation*, Vol. 14, No. 14, 302–307, 1966.

23. Liao, Z. P., H. L. Wong, B. P. Yang, and Y. F. Yuan, "A transmitting boundary for transient wave analysis," *Scientia Sinica*, Vol. 27, No. 10, 1063–1076, 1984.
24. University of Texas MD Anderson Cancer Center, "Breast cancer screening: Increased risk," available on <http://www.mdanderson.org>.
25. Flores-Tapia, D., G. Thomas, and S. Pistorius, "Skin surface removal on breast microwave imagery usng wavelet multiscale products," *Proceedings of the 5th Medical Imaging: Physiology, Function and Structure from Medical Images*, 2006.